Vietnam Journal of Mechanics, Vol. 45, No. 2 (2023), pp. 145 – 163
DOI: https://doi.org/10.15625/0866-7136/18368

PROPORTIONAL TOPOLOGY OPTIMIZATION ALGORITHM FOR TWO-SCALE CONCURRENT DESIGN OF LATTICE STRUCTURES

Minh Ngoc Nguyen[1,2,*], **Duy Vo**[1,2], **Tinh Quoc Bui**[1,2]
[1]*Duy Tan Research Institute for Computational Engineering (DTRICE) - Duy Tan University, Ho Chi Minh City 700000, Vietnam*
[2]*Faculty of Civil Engineering, Duy Tan University, Da Nang 550000, Vietnam.*
[*]E-mail: nguyenngocminh6@duytan.edu.vn

Received: 25 May 2023 / Published online: 30 June 2023

Abstract. In this paper, the Proportional Topology Optimization (PTO) algorithm is extended for the two-scale concurrent topology optimization, in which both the structure and material cellular micro-structure are subject to design. PTO was originally developed on the concept that the amount of material being distributed to an element would be proportional to the contribution of that element in the objective function. Sensitivity analysis is not required. In a two-scale concurrent topology optimization problem, two sets of design variables are defined, one for macro-structure and one for micro-structure. Here, the objective function is reformulated such that the contribution of each micro-scale design variable can be determined, facilitating the employment of PTO. The macroscopic effective elastic tensor is evaluated by the energy-based homogenization method (EBHM), providing a link between micro-structure and macro-structure. Feasibility and efficiency of the proposed PTO approach are demonstrated via several benchmark examples of both two and three dimensional structures.

Keywords: proportional topology optimization, PTO, two-scale, lattice structures.

1. INTRODUCTION

During the last decades, topology optimization has been emerging as a useful numerical tool for finding the material layout (within a pre-defined design domain) that maximizes certain performance of a given structure. The art can be traced back to the work by Bendsøe and Kikuchi [1], in which material layout was simply displayed by black (filled by material) and white (voided region). Since then, various methods have been proposed such as the Solid Isotropic Material with Penalization (SIMP) [2–5], the

Evolutionary Structural Optimization (ESO/BESO) [6,7], the Level Set Method [8,9], the Phase Field Method [10], etc. In the above methods, the design variables are usually associated with finite element mesh, either element center or nodes. Recently, the explicit techniques such as the geometry projection [11] and the Moving Morphable Components/Voids [12, 13] have been introduced. In explicit techniques, a certain number of parameterized shapes is given. Design variables are defined by the parameters of the geometric shapes and thus are independent from the finite element mesh.

In many fields of engineering, lightweight structures have been increasingly attracted attention due to many advantages such as energy effectiveness and environmental friendliness. Among them, lattice structures with repeating unit cells can be designed to achieve both lightweight and desirable properties. Not only the shape of the structure, but also the shape of the unit cell(s) (and their arrangement as well) have influence on the overall performance. Recently, many authors have explored the employment of two-scale topology optimization in design of lattice structures, such that both the topology of the macro-scale structure and the micro-scale structure (the unit cell) are simultaneously optimized [14–18]. Two finite element models are established, one for each structure. Based on the design of micro-scale unit cell, the macroscopic effective properties would be evaluated by homogenization techniques. The macro-scale structure is assumed to be homogeneous, in which material properties are taken as the homogenized properties. Both theoretical and numerical implementation aspects of homogenization have been thoroughly discussed in various published works, for e.g. see [17, 19–22]. Influence of arrangement of unit cells could be taken into account, by considering the angle of orientation as additional design variables [15, 23]. The existence of multiple -structures has also been considered by various authors [16, 24–26]. In such cases, connectivity between adjacent cells of different types is usually not available and has to be enforced [16, 25]. Alternatively, interface layer is defined [26].

Most of the works on topology optimization available in the literatures are based on sensitivity analysis. The sensitivity information, i.e. the derivatives of objective function and constraints with respect to design variables, is required to update the design. On the other hand, there exist alternative methods do not need the calculation of sensitivity. Early attempts rely on black/white (0/1) representation of material layout and meta-heuristic search algorithms such as ant colony algorithm, genetic algorithm, particle swarm optimization, etc. [27–29]. This approach was criticized for inefficiency [30]. Although a search algorithm is expected to overcome local optimum, it does not guarantee that a global optimum can be achieved. Even when there are only two options for each element, 0 or 1, the number of possible combinations would be 2^N for a mesh of N finite elements. Therefore, the searching space is quickly scaled up when a fine mesh is used, tremendously increasing the computational cost. Recently, Guirguis et al [31, 32]

introduced a level-set approach without calculation of sensitivity, in which the evolution of level set function is updated by pattern search algorithm. The concept of cellular automata was employed by various authors for topology optimization of many problem types: minimum compliance [33], design of materials [34], and two-scale concurrent optimization [24]. In this concept, design variable in each element is updated by comparing strain energy value with other elements within a pre-defined neighborhood. The Proportional Topology Optimization (PTO) algorithm was originally developed by Biyikli and To [35] for volume-constrained compliance minimization and stress-constrained mass minimization problems. The core idea of PTO method is quite simple: the amount of material distributed into each element is proportional to the contribution of that element in the objective function (for e.g. the structural compliance). Wang et al. [36] proposed an improvement on update scheme of PTO for minimum compliance problems. The stress-constrained mass minimization by PTO was further discussed by Cheng et al. [37] and Ullah et al. [38]. Wang et al. [39] later included loading uncertainty into PTO procedure. A version of PTO for multi-material problems was also freshly developed by Nguyen et al. for compliance problems [40] and compliant mechanism problems [41], with the aid of the Alternative Active Phase Algorithm (AAPA) [42]. An attempt on hybrid approach for two-scale topology optimization was discussed in [43], such that PTO algorithm was employed for macro-scale structure while the common Optimality Criteria (OC) algorithm was used for design of micro-scale structure.

In this paper, the PTO algorithm is further extended for both scales of the two-scale concurrent design of lattice structures. The key point is design of micro-structure by PTO. To do that, the contribution of each micro-domain element in the objective function (the compliance of macro-structure has to be determined. The macroscopic effective elastic tensor is numerically evaluated using the energy-based homogenization method.

The paper is organized as follows. Right after the Introduction is a brief on the Energy-based homogenization method in Section **2**. Section **3** is reserved for the formulation of PTO algorithm for the two-scale topology optimization. Several numerical examples are investigated in Section **4** to demonstrate the capability of the proposed approach. Finally, some concluding remarks are given in Section **5**.

2. ENERGY-BASED HOMOGENIZATION METHOD (EBHM)

Within the scope of linear elasticity, the macroscopic effective elastic tensor can be estimated through homogenization techniques being applied on a micro-scale unit cell (micro-structure) [19]. For better accuracy, the following two assumptions have to be satisfied: (i) the micro-structure is periodically distributed within the macro-structure,

and (ii) the bulk size of the macro-scale structure is much larger than that of the micro-structure. Here, the estimation is numerically conducted via the energy-based homogenization method (EBHM) [17, 22]. Assuming that the micro-scale unit cell is defined within a square domain Ω_m, the homogenized elastic tensor can be computed by

$$\mathbf{D}^H = \frac{1}{|\Omega_m|}\int_{\Omega^m} \left(\boldsymbol{\varepsilon}\left(\mathbf{u}_m^0\right) - \boldsymbol{\varepsilon}\left(\mathbf{u}_m\right)\right)^T \mathbf{D}_m \left(\boldsymbol{\varepsilon}\left(\mathbf{u}_m^0\right) - \boldsymbol{\varepsilon}\left(\mathbf{u}_m\right)\right) \mathrm{d}\Omega_m, \tag{1}$$

where $\mathbf{D}_m$ is the local varying elastic tensor and $\boldsymbol{\varepsilon}(\mathbf{u}_m^0)$ is the linearly independent unit test strain field. Note that subscript m is used throughout this paper to indicate that a quantity belongs to the micro-structure. $\boldsymbol{\varepsilon}(\mathbf{u}_m)$ is the unknown strain field within the unit cell, and can be determined by solving the equilibrium equation (see Eq. (6)) with periodic boundary condition [17, 22]. By using SIMP [4, 5], the tensor $\mathbf{D}_m$ is computed as

$$\mathbf{D}_m(\rho_{m,j}) = \left(k + (1-k)\rho_{m,j}^p\right)\mathbf{D}_0, \tag{2}$$

where $\mathbf{D}_0$ is the elastic tensor of the base material and $\rho_{m,j}$ is the design variable associated with the j^{th} element of the micro-structure domain. k is a very small positive value that is chosen to avoid zero stiffness when $\rho_{m,j} \approx 0$, and p is the penalization number.

3. FORMULATION FOR THE TWO-SCALE TOPOLOGY OPTIMIZATION BY THE PTO ALGORITHM

3.1. Problem statement for compliance minimization

The two-scale concurrent topology optimization for minimum compliance of macro-structure can be mathematically stated as follows

$$\text{Find} \quad : \quad \rho_i \in [0,1],\ \rho_{m,j} \in [0,1],\ (i = 1,2,3,\ldots,N)\,,\ (j = 1,2,3,\ldots,N_m) \tag{3}$$

$$\text{Objective} \quad : \quad \text{minimize}\ c = \int_{\Omega} \left(\boldsymbol{\varepsilon}\left(\mathbf{u}\right)\right)^T \mathbf{D}\boldsymbol{\varepsilon}\left(\mathbf{u}\right)\mathrm{d}\Omega = \mathbf{u}^T\mathbf{K}\mathbf{u}, \tag{4}$$

subject to

$$\mathbf{K}\mathbf{u} = \mathbf{F}, \tag{5}$$

$$\int_{\Omega^m} \left(\boldsymbol{\varepsilon}\left(\delta\mathbf{u}_m\right)\right)^T \mathbf{D}_m\boldsymbol{\varepsilon}\left(\mathbf{u}_m\right)\mathrm{d}\Omega_m = \int_{\Omega^m} \left(\boldsymbol{\varepsilon}\left(\delta\mathbf{u}_m\right)\right)^T \mathbf{D}_m\boldsymbol{\varepsilon}\left(\mathbf{u}_m^0\right)\mathrm{d}\Omega_m, \tag{6}$$

$$\int_{\Omega} \rho \mathrm{d}\Omega = \sum_i \rho_i V_i \le \bar{v}|\Omega|, \tag{7}$$

$$\int_{\Omega_m} \rho_m \mathrm{d}\Omega_m = \sum_i \rho_{m,i} V_{m,i} \le \bar{v}_m|\Omega_m|. \tag{8}$$

Here, the design variables (pseudo-density values ρ_i for macro-scale and $\rho_{m,j}$ for micro-scale) are defined at the element center. Thus the number of design variables (N and N_m) are equal to the number of elements. The compliance in Eq. (4) is a measure of elastic strain energy. $\mathbf{u}$ is the displacement vector of the macro-structure, and can be obtained by solving the equilibrium in Eq. (5), in which $\mathbf{K}$ is the stiffness matrix and $\mathbf{F}$ is the load vector. Eq. (6) is the equilibrium in micro-structure, in which $\delta\mathbf{u}_m$ is the test function that satisfies the requirement for finite element analysis. Eq. (7) and Eq. (8) are the volume constraint for the macro-structure and micro-structure, respectively. V_i and $V_{m,j}$ denote the volume of element (or area for 2D domain) in macro- and micro-scale, while $\bar{v}$ and $\bar{v}_m$ are the given volume fractions.

Via finite element analysis, the (macro-scale) global stiffness matrix $\mathbf{K}$ in Eq. (4) is computed by

$$\mathbf{K} = \sum_{i=1}^{N} \mathbf{K}_{e,i}, \tag{9}$$

The stiffness matrix of each element i, $\mathbf{K}_{e,i}$, is given by

$$\mathbf{K}_{e,i} = \int_{\Omega^{e,i}} \mathbf{B}^T \mathbf{D}(\rho_i) \mathbf{B} \mathrm{d}\Omega, \tag{10}$$

where $\mathbf{B}$ denotes the operator to calculate the components of strain tensor $\boldsymbol{\varepsilon}$, such that $\boldsymbol{\varepsilon}(\mathbf{u}_{e,i}) = \mathbf{B}\mathbf{u}_{e,i}$, and $\mathbf{u}_{e,i}$ is the vector of nodal displacement of element i. $\mathbf{D}(\rho_i)$ is the elastic tensor with respect to the (pseudo) density, which is calculated using the SIMP technique as

$$\mathbf{D}(\rho_i) = \left(k + (1-k)\rho_i^p\right) \mathbf{D}^H, \tag{11}$$

where $\mathbf{D}^H$ is determined from Eq. (1).

3.2. PTO algorithm for macro-scale design variables

The PTO algorithm was originally introduced by Biyikli and To [35], such that material would be distributed into an arbitrary element proportionally to the contribution of that element in the objective function. For the problem of minimum compliance, elements with high value of compliance (high value of elastic strain energy) would receive more amount of material than elements with low value of compliance. Within the framework of finite element analysis, it was implied in [35] that one pseudo-density (design variable) was defined for each element (at the element center). However, the idea could be extended for other ways of defining design variables, for e.g. when meshfree analysis [38, 44] or virtual element method [45] is employed instead of conventional finite element analysis.

By finite element analysis, the structural compliance in Eq. (4) can be written as a sum of elemental values

$$c = \sum_{i=1}^{N} c_i, \tag{12}$$

$$c_i = \mathbf{u}_{e,i}^T \mathbf{K}_{e,i} \mathbf{u}_{e,i}. \tag{13}$$

Material is distributed into element i by

$$\hat{\rho}_i = \hat{\rho}_i + \Delta\hat{\rho}_i, \quad \hat{\rho}_i \in [0,1] \tag{14}$$

$$\Delta\hat{\rho}_i = RM \frac{c_i}{\sum_{k=1}^{N} c_k V_k}, \tag{15}$$

In order to avoid checkerboard, a density filter is applied as follows

$$\rho_i = \frac{\sum w_{ik}\hat{\rho}_k}{\sum w_{ik}}, \tag{16}$$

in which the weight coefficient $w_{ik} > 0$ can be determined by a decay function with respect to the distance between the center points of element i and element k. For more details, readers are referred to Refs. [4,5,35]. RM in Eq. (15) denotes the *remaining amount of material*. At the beginning of the PTO loop, RM is taken as the *total amount of material* TM, which is defined by the constraint in Eq. (7), i.e. $RM = TM = \bar{v}|\Omega|$. Via the PTO loop, RM is updated by $RM = RM - \sum \rho_i V_i$. The loop stops when RM is less than a predefined value, for e.g. $RM \leq 0.001\ TM$. After the PTO loop, the density value can be further blended with history value to enhance convergence

$$\rho_{t+1} = \alpha\rho_t + (1-\alpha)\rho^{PTO}, \tag{17}$$

where ρ_{t+1} is the density value at current iteration, ρ_t is the density value at previous iteration and ρ^{PTO} is the density value calculated by PTO algorithm. Coefficient α controls the weight of ρ_t and ρ^{PTO}. No update occurs if $\alpha = 1$, while history value has no effect if $\alpha = 0$. In this paper, $\alpha = 0.5$ is selected.

3.3. PTO algorithm for micro-scale design variables

In order to employ PTO algorithm for updating micro-scale design variables, it is essential to calculate the contribution of each element j (of the micro-structure) in the compliance given in Eq. (4). Substituting Eq. (10) and Eq. (11) into Eq. (13) reads

$$c_i = \mathbf{u}_{e,i}^T \left(\int_{\Omega^{e,i}} \mathbf{B}^T \left(k + (1-k)\rho_i^p\right) \mathbf{D}^H \mathbf{B} \mathrm{d}\Omega \right) \mathbf{u}_{e,i}. \tag{18}$$

The homogenized elastic tensor $\mathbf{D}^H$ in Eq. (1) is given by an integral over the micro-scale domain. By numerical integration, $\mathbf{D}^H$ can thus be computed as a sum of elemental values, i.e.

$$\mathbf{D}^H = \sum_{j=1}^{N_m} \mathbf{D}^H_{m,j}. \tag{19}$$

Therefore the structural compliance can be written by

$$c = \sum_{i=1}^{N} c_i = \sum_{i=1}^{N} \mathbf{u}^T_{e,i} \left(\int_{\Omega^{e,i}} \mathbf{B}^T \left(k + (1-k)\rho_i^p\right) \left(\sum_{j=1}^{N_m} \mathbf{D}^H_{m,j} \right) \mathbf{B} \mathrm{d}\Omega \right) \mathbf{u}_{e,i} \tag{20}$$

Rearranging Eq. (20) leads to

$$c = \sum_{j=1}^{N_m} \left(\sum_{i=1}^{N} \mathbf{u}^T_{e,i} \left(\int_{\Omega^{e,i}} \mathbf{B}^T \left(k + (1-k)\rho_i^p\right) \mathbf{D}^H_j \mathbf{B} \mathrm{d}\Omega \right) \mathbf{u}_{e,i} \right) = \sum_{j=1}^{N_m} c_{m,j}, \tag{21}$$

$$c_{m,j} = \sum_{i=1}^{N} \mathbf{u}^T_{e,i} \left(\int_{\Omega^{e,i}} \mathbf{B}^T \left(k + (1-k)\rho_i^p\right) \mathbf{D}^H_{m,j} \mathbf{B} \mathrm{d}\Omega \right) \mathbf{u}_{e,i}. \tag{22}$$

The contribution of each micro-scale element j is given in Eq. (22) and could be interpreted as the elastic strain energy of the macro-structure when $\mathbf{D}^H_{m,j}$ is taken as the elastic tensor. Once the contribution of each micro-scale element is computed via Eq. (22), it is possible to update the micro-scale (pseudo) density by the PTO algorithm as described in Section **3.2**.

Calculation of Eq. (22) requires a domain integral over the micro-structure domain, and this process has to be conducted for every micro-scale element j. It is noticed that the integral in Eq. (22) has the same form with that of the element stiffness matrix $\mathbf{K}_{e,i}$ in Eq. (10), in which $\mathbf{D}^H$ is replaced by $\mathbf{D}^H_{m,j}$. This observation could be exploited for efficient implementation [43].

4. NUMERICAL EXAMPLES

For demonstration of the proposed approach (PTO algorithm for two-scale design by topology optimization), four benchmark examples including a cantilever beam, an annular cylinder being tangentially loaded, a three-dimensional support structure, and a three-dimensional beam under torsional forces. Without loss of generality, an artificial material with elastic modulus $E = 1$ MPa and Poisson's ration $\nu = 0.3$ is selected in numerical analysis. Initially, the configuration of both macro- and macro-scale domain are as follows (see Fig. 1 for illustration):

- Macro-scale domain: the value of every design variable is equal to the required volume fraction.
- Micro-scale domain: the value of every design variable is equal to one, except for the hole at the center of the domain which is voided region.

For stopping criterion of optimization process, it is required that changes of designs in both scales must not exceed 1%.

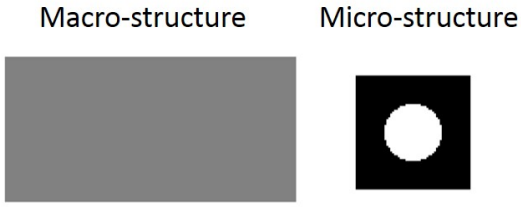

Fig. 1. Illustration of initial configurations. The design domain for macro-structure will be specified for each numerical example, while the design domain for micro-structure is a square domain of size 0.1×0.1 mm. In three-dimensional (3D) case(s), the design domain for micro-structure is a cube of size $0.1 \times 0.1 \times 0.1$ mm with a spherical hole at center. For finite element analysis, a mesh of 60×60 four-node quadrilateral elements is used for the 2D micro-scale domain, while a mesh of $20 \times 20 \times 20$ eight-node brick elements is used for the 3D micro-scale domain

4.1. Two-scale design of a doubly clamped beam

In this example, design of a doubly clamped beam being loaded by multiple concentrated forces, as depicted in Fig. 2. A mesh of 120×30 four-node quadrilateral elements is used to discretize the beam domain.

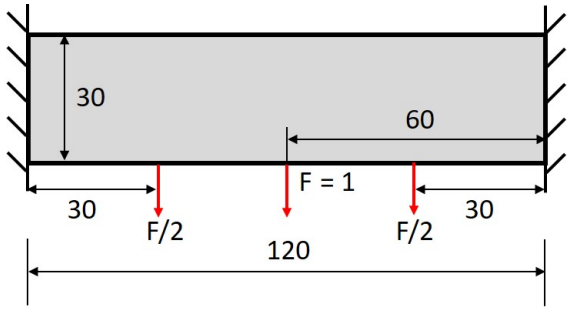

Fig. 2. Schematic sketch of a doubly clamped beam being loaded by multiple concentrated forces

Fig. 3 presents the designs by PTO for two cases: (Case 1) volume fraction of the macro-domain is $\bar{v} = 60\%$ and volume fraction the micro-domain is $\bar{v}_m = 40\%$, and (Case 2) $\bar{v} = 40\%$ and $\bar{v}_m = 40\%$. The shape of the two designs shares some similarities.

Due to smaller volume fraction, the macro-structure in Case 2 has smaller thickness and does not have upper part. The history curves of the compliance values of the two designs are depicted in Fig. 4.

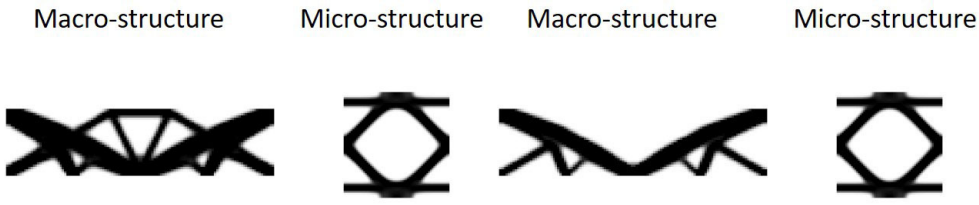

$$\mathbf{D}_H = \begin{bmatrix} 0.2132 & 0.0678 & 0.0000 \\ 0.0678 & 0.0848 & 0.0000 \\ 0.0000 & 0.0000 & 0.0680 \end{bmatrix}$$

(a) Case 1: $\bar{v} = 60\%$, $\bar{v}_m = 40\%$

$$\mathbf{D}_H = \begin{bmatrix} 0.2276 & 0.0646 & 0.0000 \\ 0.0678 & 0.0780 & 0.0000 \\ 0.0000 & 0.0000 & 0.0658 \end{bmatrix}$$

(b) Case 2: $\bar{v} = 40\%$, $\bar{v}_m = 40\%$

Fig. 3. Designs by PTO for two cases

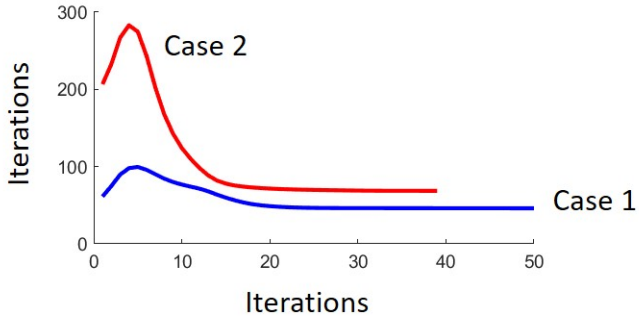

Fig. 4. History curves of compliance values of the two designs in Fig. 3

4.2. Two-scale design of an annular cylinder being tangentially loaded

The problem of an annular cylinder being tangentially loaded, as sketched in Fig. 5, is studied in this example. Fig. 6 presents a comparison between three approaches: OC algorithm for both scales, hybrid approach (PTO for macro-structure and OC for micro-structure) [43], and the proposed approach in this study - PTO algorithm for both scales. There are slight differences in the three designs, leading to different values of compliance. The lowest value of compliance is obtained by the proposed approach. History curves of compliance are presented in Fig. 7. It is interesting that computational time decreases when PTO replaces OC in macro-scale design (case b)), and when PTO replaces OC in

both scales (case c)). The reason is probably due to less number of iterations, as the average time needed for each iteration is almost equivalent between PTO and OC [41].

In this paper, no projection technique is adopted to push the density values close to 0 or 1. Hence, grey regions (i.e., elements with intermediate density values) can be observed in Fig. 6. Based on suggestion of Ref. [46], the measure of non-discreteness is calculated as

$$M_{nd} = \frac{\sum_{e=1}^{NE} 4\rho_e(1-\rho_e)}{NE} \times 100\%, \tag{23}$$

where ρ_e is the (filtered) density value at element e and NE is the number of elements. The value of M_{nd} would be 100% if the domain is totally grey, i.e. the density values are all equal to 0.5. The lower the value of M_{nd} is, the lower the non-discreteness is. $M_{nd} = 0\%$ indicates that the result is indeed binary, i.e. the element density is either 0 or 1 for all elements. As reported in Table 1, the non-discreteness values for all the three cases are almost equivalent.

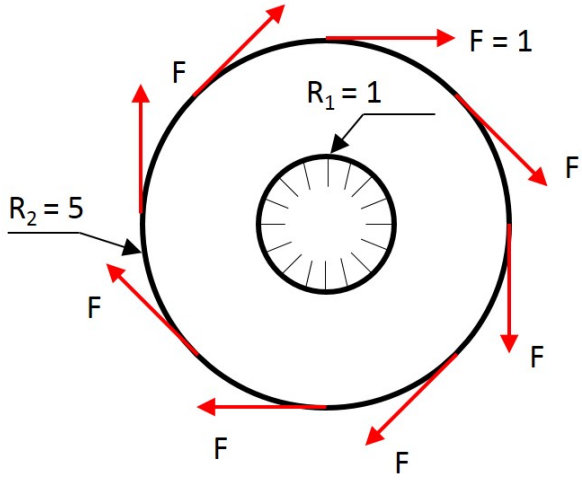

Fig. 5. Schematic sketch of an annular cylinder being tangentially loaded

Table 1. The measure of non-discreteness evaluated for the three cases of Fig. 6

	OC	Hybrid	PTO
Macro-structure	28.7%	27.2%	27.2%
Micro-structure	22.1%	22.3%	22.9%

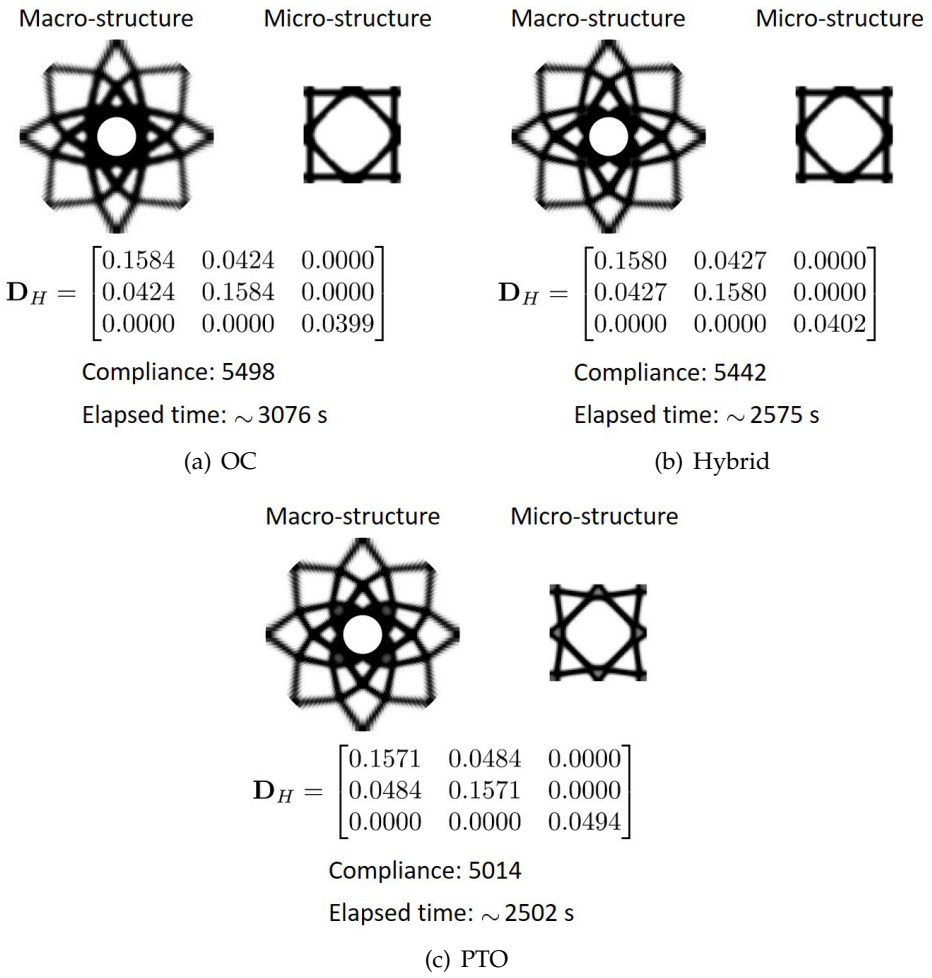

Fig. 6. Design obtained by three approaches: a) OC for both scales, b) Hybrid approach (PTO for macro-structure, and OC for micro-structure) [43], and c) PTO algorithm for both scales

4.3. Two-scale design of a three-dimensional (3D) supported structure

In this example, the proposed PTO approach is employed for design of a three-dimensional supported structure, as depicted in Fig. 8. Comparison between the three approaches (OC algorithm, Hybrid approach, and PTO algorithm) in Fig. 9 again exhibits that a design with lowest value of compliance can be obtained by PTO. For a closer look, the measure of non-discreteness for the three designs are reported in Table 2. In this particular problem, the non-discreteness of PTO design is a little bit better than that of the other two counterparts. The PTO algorithm also requires less number of iterations than the other two approaches, as depicted in Fig. 10.

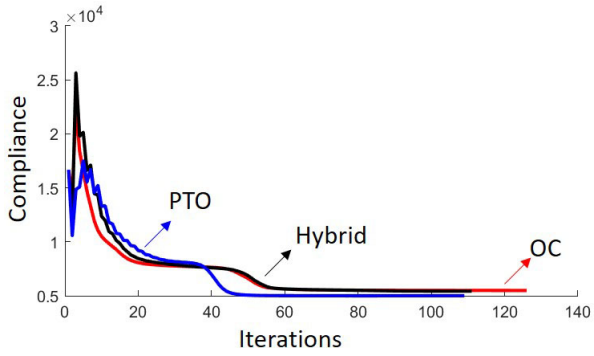

Fig. 7. History curves of compliance values for the three designs in Fig. 6

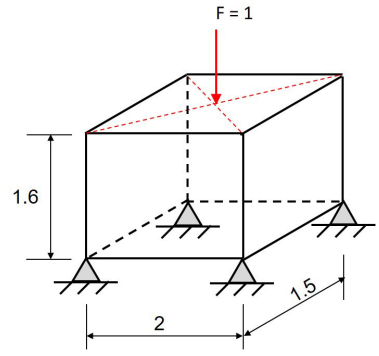

Fig. 8. Schematic sketch of a 3D-supported structure

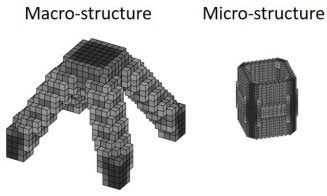

$$\mathbf{D}_H = \begin{bmatrix} 0.0550 & 0.0309 & 0.0498 & 0 & 0 & 0 \\ 0.0309 & 0.1775 & 0.0309 & 0 & 0 & 0 \\ 0.0498 & 0.0309 & 0.0550 & 0 & 0 & 0 \\ 0 & 0 & 0 & 0.0343 & 0 & 0 \\ 0 & 0 & 0 & 0 & 0.0343 & 0 \\ 0 & 0 & 0 & 0 & 0 & 0.0442 \end{bmatrix}$$

Compliance: 377.2858

(a) OC

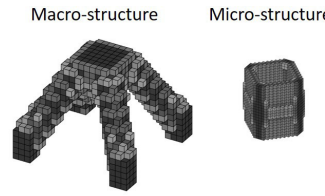

$$\mathbf{D}_H = \begin{bmatrix} 0.0550 & 0.0309 & 0.0498 & 0 & 0 & 0 \\ 0.0309 & 0.1775 & 0.0309 & 0 & 0 & 0 \\ 0.0498 & 0.0309 & 0.0550 & 0 & 0 & 0 \\ 0 & 0 & 0 & 0.0343 & 0 & 0 \\ 0 & 0 & 0 & 0 & 0.0343 & 0 \\ 0 & 0 & 0 & 0 & 0 & 0.0442 \end{bmatrix}$$

Compliance: 361.7062

(b) Hybrid

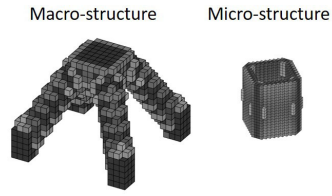

$$\mathbf{D}_H = \begin{bmatrix} 0.0619 & 0.0358 & 0.0571 & 0 & 0 & 0 \\ 0.0358 & 0.1928 & 0.0358 & 0 & 0 & 0 \\ 0.0571 & 0.0358 & 0.0619 & 0 & 0 & 0 \\ 0 & 0 & 0 & 0.0385 & 0 & 0 \\ 0 & 0 & 0 & 0 & 0.0385 & 0 \\ 0 & 0 & 0 & 0 & 0 & 0.0477 \end{bmatrix}$$

Compliance: 325.9966

(c) PTO

Fig. 9. Design obtained by three approaches: a) OC algorithm, b) Hybrid approach [43], and c) PTO algorithms for the 3D supported structure. Volume fraction: $\bar{v} = 20\%$ and $\bar{v}_m = 30\%$

Table 2. The measure of non-discreteness evaluated for the three cases in Fig. 9

	OC	Hybrid	PTO
Macro-structure	21.9%	16.2%	16.1%
Micro-structure	36.0%	36.0%	34.2%

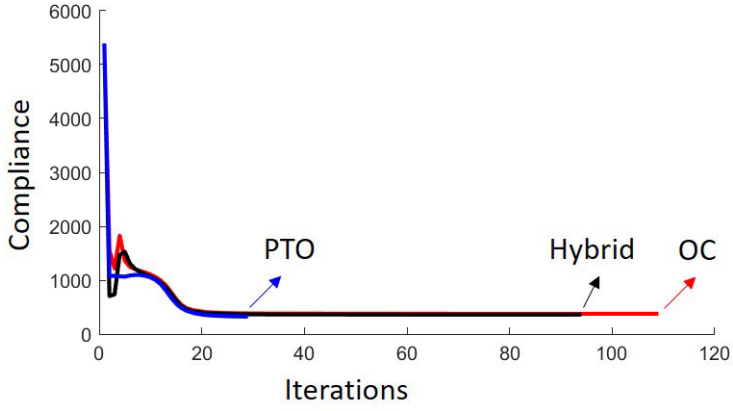

Fig. 10. History curves of compliance values for the three designs in Fig. 9

4.4. Two-scale design of a 3D cantilever beam subjected to torsional forces

The two-scale design of 3D beam, as depicted in Fig. 11, is investigated in this example. One end of the beam is clamped, while the other end is subjected to torsional forces. Given the volume fraction of macro-scale structure as $\bar{v} = 20\%$ and that of micro-scale structure as $\bar{v}_m = 30\%$, the design by PTO is depicted in Fig. 12. The corresponding history curve of compliance value is presented in Fig. 13, in which the evolution of the results are also included, clearly showing that both scales are simultaneously optimized.

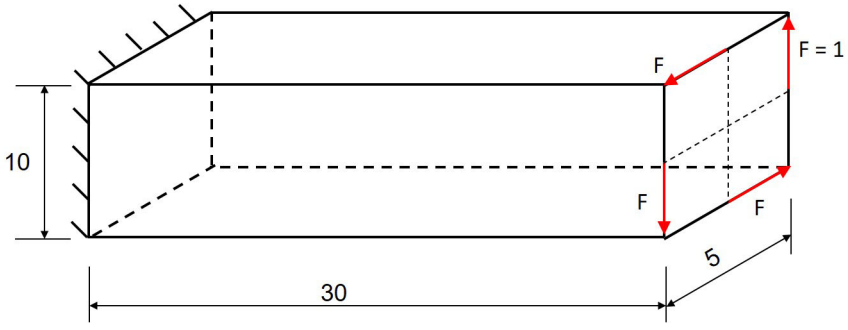

Fig. 11. Schematic sketch of a 3D beam subjected to torsional forces

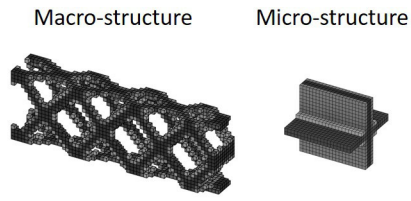

$$\mathbf{D}_H = \begin{bmatrix} 0.2352 & 0.0504 & 0.0346 & 0 & 0 & 0 \\ 0.0504 & 0.1576 & 0.0103 & 0 & 0 & 0 \\ 0.00346 & 0.0103 & 0.1051 & 0 & 0 & 0 \\ 0 & 0 & 0 & 0.0554 & 0 & 0 \\ 0 & 0 & 0 & 0 & 0.0023 & 0 \\ 0 & 0 & 0 & 0 & 0 & 0.0371 \end{bmatrix}$$

Compliance: 4361

Fig. 12. Design obtained by PTO algorithms for cantilever beam subjected to torsional forces. Volume fraction: $\bar{v} = 20\%$ and $\bar{v}_m = 30\%$

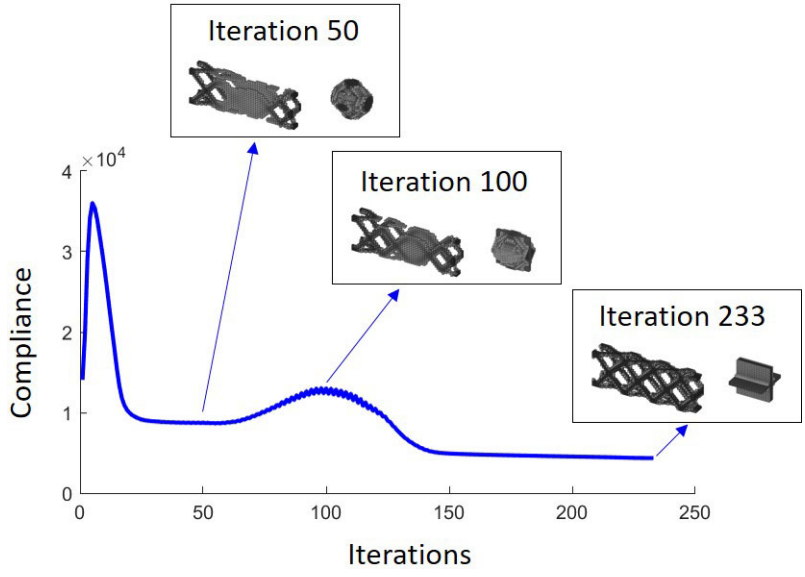

Fig. 13. History curve of compliance value for the design in Fig. 12

5. CONCLUSIONS

The PTO algorithm has been successfully extended for both scales of the two-scale topology optimization for design of lattice structures. The main contribution of this study is that the objective function (the structural compliance) is mathematically transformed to enable the application of PTO algorithm to update the micro-scale design variables. Via

several numerical examples, performance of the proposed approach have been demonstrated. It is also shown that the proposed approach is capable for both two- and three-dimensional problems. As PTO algorithm for design of compliant mechanisms has been recently introduced [41, 45], the two-scale concurrent design of compliant mechanisms by PTO could also be conducted without much difficulty. A remedy to reduce the grey zone and boost the discreteness of the optimized results would be the employment of Heaviside-type projection [47, 48]. Adaptation of the volume-preserving Heaviside projection technique into PTO algorithm has been discussed in [37, 45].

The current work would facilitate further research on application of PTO algorithm for design of micro-structures with desired homogenized properties based on the EBHM method [22]. Another possible extension that could be investigated in future works is the consideration of multiple micro-structures. In that case, the connection between different micro-structures has to be taken into account [16, 49].

A drawback of the current formulation is that it does not take the effect of micro-structure size on deformation into account. In fact, there exist some attempts to consider the size-dependent effect in topology optimization, for e.g. using strain gradient theory [50] or couple stress theory [51, 52]. This would be an interesting extension for future works on design of lattice structures by multi-scale topology optimization.

DECLARATION OF COMPETING INTEREST

The authors declare that they have no known competing financial interests or personal relationships that could have appeared to influence the work reported in this paper.

FUNDING

This research received no specific grant from any funding agency in the public, commercial, or not-for-profit sectors.

REFERENCES

[1] M. P. Bendsøe and N. Kikuchi. Generating optimal topologies in structural design using a homogenization method. *Computer Methods in Applied Mechanics and Engineering*, **71**, (1988), pp. 197–224. https://doi.org/10.1016/0045-7825(88)90086-2.

[2] H. P. Mlejnek. Some aspects of the genesis of structures. *Structural Optimization*, **5**, (1-2), (1992), pp. 64–69. https://doi.org/10.1007/bf01744697.

[3] M. P. Bendsøe and O. Sigmund. Material interpolation schemes in topology optimization. *Archive of Applied Mechanics (Ingenieur Archiv)*, **69**, (9-10), (1999), pp. 635–654. https://doi.org/10.1007/s004190050248.

[4] O. Sigmund. A 99 line topology optimization code written in Matlab. *Structural and Multidisciplinary Optimization*, **21**, (2), (2001), pp. 120–127. https://doi.org/10.1007/s001580050176.

[5] E. Andreassen, A. Clausen, M. Schevenels, B. S. Lazarov, and O. Sigmund. Efficient topology optimization in MATLAB using 88 lines of code. *Structural and Multidisciplinary Optimization*, **43**, (1), (2010), pp. 1–16. https://doi.org/10.1007/s00158-010-0594-7.

[6] Y. M. Xie and G. P. Steven. A simple evolutionary procedure for structural optimization. *Computers & Structures*, **49**, (5), (1993), pp. 885–896. https://doi.org/10.1016/0045-7949(93)90035-c.

[7] X. Huang and Y. M. Xie. Bi-directional evolutionary topology optimization of continuum structures with one or multiple materials. *Computational Mechanics*, **43**, (3), (2009), pp. 393–401. https://doi.org/10.1007/s00466-008-0312-0.

[8] M. Y. Wang, X. Wang, and D. Guo. A level set method for structural topology optimization. *Computer Methods in Applied Mechanics and Engineering*, **192**, (1-2), (2003), pp. 227–246. https://doi.org/10.1016/s0045-7825(02)00559-5.

[9] G. Allaire, F. Jouve, and A.-M. Toader. Structural optimization using sensitivity analysis and a level-set method. *Journal of Computational Physics*, **194**, (1), (2004), pp. 363–393. https://doi.org/10.1016/j.jcp.2003.09.032.

[10] A. Takezawa, S. Nishiwaki, and M. Kitamura. Shape and topology optimization based on the phase field method and sensitivity analysis. *Journal of Computational Physics*, **229**, (7), (2010), pp. 2697–2718. https://doi.org/10.1016/j.jcp.2009.12.017.

[11] J. A. Norato, B. K. Bell, and D. A. Tortorelli. A geometry projection method for continuum-based topology optimization with discrete elements. *Computer Methods in Applied Mechanics and Engineering*, **293**, (2015), pp. 306–327. https://doi.org/10.1016/j.cma.2015.05.005.

[12] X. Guo, W. Zhang, and W. Zhong. Doing topology optimization explicitly and geometrically—a new moving morphable components based framework. *Journal of Applied Mechanics*, **81**, (8), (2014). https://doi.org/10.1115/1.4027609.

[13] W. Zhang, D. Li, J. Zhou, Z. Du, B. Li, and X. Guo. A Moving Morphable Void (MMV)-based explicit approach for topology optimization considering stress constraints. *Computer Methods in Applied Mechanics and Engineering*, **334**, (2018), pp. 381–413. https://doi.org/10.1016/j.cma.2018.01.050.

[14] X. Yan, X. Huang, Y. Zha, and Y. M. Xie. Concurrent topology optimization of structures and their composite microstructures. *Computers & Structures*, **133**, (2014), pp. 103–110. https://doi.org/10.1016/j.compstruc.2013.12.001.

[15] X. Gao and H. Ma. A modified model for concurrent topology optimization of structures and materials. *Acta Mechanica Sinica*, **31**, (2015), pp. 890–898. https://doi.org/10.1007/s10409-015-0502-x.

[16] H. Li, Z. Luo, L. Gao, and Q. Qin. Topology optimization for concurrent design of structures with multi-patch microstructures by level sets. *Computer Methods in Applied Mechanics and Engineering*, **331**, (2018), pp. 536–561. https://doi.org/10.1016/j.cma.2017.11.033.

[17] J. Gao, Z. Luo, L. Xia, and L. Gao. Concurrent topology optimization of multiscale composite structures in Matlab. *Structural and Multidisciplinary Optimization*, **60**, (6), (2019), pp. 2621–2651. https://doi.org/10.1007/s00158-019-02323-6.

[18] C. Zhuang, Z. Xiong, and H. Ding. Bézier extraction based isogeometric approach to multi-objective topology optimization of periodic microstructures. *International Journal for Numerical Methods in Engineering*, **122**, (2021), pp. 6827–6866. https://doi.org/10.1002/nme.6813.

[19] J. Guedes and N. Kikuchi. Preprocessing and postprocessing for materials based on the homogenization method with adaptive finite element methods. *Computer Methods in Applied Mechanics and Engineering*, **83**, (2), (1990), pp. 143–198. https://doi.org/10.1016/0045-7825(90)90148-f.

[20] O. Sigmund. Materials with prescribed constitutive parameters: An inverse homogenization problem. *International Journal of Solids and Structures*, **31**, (17), (1994), pp. 2313–2329. https://doi.org/10.1016/0020-7683(94)90154-6.

[21] E. Andreassen and C. S. Andreasen. How to determine composite material properties using numerical homogenization. *Computational Materials Science*, **83**, (2014), pp. 488–495. https://doi.org/10.1016/j.commatsci.2013.09.006.

[22] L. Xia and P. Breitkopf. Design of materials using topology optimization and energy-based homogenization approach in Matlab. *Structural and Multidisciplinary Optimization*, **52**, (6), (2015), pp. 1229–1241. https://doi.org/10.1007/s00158-015-1294-0.

[23] Y. Lu and L. Tong. Concurrent topology optimization of cellular structures and anisotropic materials. *Computers & Structures*, **255**, (2021). https://doi.org/10.1016/j.compstruc.2021.106624.

[24] J. Jia, D. Da, C.-L. Loh, H. Zhao, S. Yin, and J. Xu. Multiscale topology optimization for non-uniform microstructures with hybrid cellular automata. *Structural and Multidisciplinary Optimization*, **62**, (2), (2020), pp. 757–770. https://doi.org/10.1007/s00158-020-02533-3.

[25] P. Liu, Z. Kang, and Y. Luo. Two-scale concurrent topology optimization of lattice structures with connectable microstructures. *Additive Manufacturing*, **36**, (2020). https://doi.org/10.1016/j.addma.2020.101427.

[26] X. Gu, S. He, Y. Dong, and T. Song. An improved ordered SIMP approach for multiscale concurrent topology optimization with multiple microstructures. *Composite Structures*, **287**, (2022). https://doi.org/10.1016/j.compstruct.2022.115363.

[27] G.-C. Luh and C.-Y. Lin. Structural topology optimization using ant colony optimization algorithm. *Applied Soft Computing*, **9**, (2009), pp. 1343–1353. https://doi.org/10.1016/j.asoc.2009.06.001.

[28] D. Sharma, K. Deb, and N. N. Kishore. Domain-specific initial population strategy for compliant mechanisms using customized genetic algorithm. *Structural and Multidisciplinary Optimization*, **43**, (2010), pp. 541–554. https://doi.org/10.1007/s00158-010-0575-x.

[29] G.-C. Luh, C.-Y. Lin, and Y.-S. Lin. A binary particle swarm optimization for continuum structural topology optimization. *Applied Soft Computing*, **11**, (2011), pp. 2833–2844. https://doi.org/10.1016/j.asoc.2010.11.013.

[30] O. Sigmund. On the usefulness of non-gradient approaches in topology optimization. *Structural and Multidisciplinary Optimization*, **43**, (2011), pp. 589–596. https://doi.org/10.1007/s00158-011-0638-7.

[31] D. Guirguis and M. F. Aly. A derivative-free level-set method for topology optimization. *Finite Elements in Analysis and Design*, **120**, (2016), pp. 41–56. https://doi.org/10.1016/j.finel.2016.06.002.

[32] D. Guirguis, W. W. Melek, and M. F. Aly. High-resolution non-gradient topology optimization. *Journal of Computational Physics*, **372**, (2018), pp. 107–125. https://doi.org/10.1016/j.jcp.2018.06.025.

[33] B. Bochenek and K. Tajs-Zielińska. GOTICA - generation of optimal topologies by irregular cellular automata. *Structural and Multidisciplinary Optimization*, **55**, (2017), pp. 1989–2001. https://doi.org/10.1007/s00158-016-1614-z.

[34] D. C. Da, J. H. Chen, X. Y. Cui, and G. Y. Li. Design of materials using hybrid cellular automata. *Structural and Multidisciplinary Optimization*, **56**, (1), (2017), pp. 131–137. https://doi.org/10.1007/s00158-017-1652-1.

[35] E. Biyikli and A. C. To. Proportional topology optimization: a new non-sensitivity method for solving stress constrained and minimum compliance problems and its implementation in MATLAB. *PLOS ONE*, **10**, (12), (2015). https://doi.org/10.1371/journal.pone.0145041.

[36] H. Wang, W. Cheng, R. Du, S. Wang, and Y. Wang. Improved proportional topology optimization algorithm for solving minimum compliance problem. *Structural and Multidisciplinary Optimization*, **62**, (2), (2020), pp. 475–493. https://doi.org/10.1007/s00158-020-02504-8.

[37] W. Cheng, H. Wang, M. Zhang, and R. Du. Improved proportional topology optimization algorithm for minimum volume problem with stress constraints. *Engineering Computations*, **38**, (2020), pp. 392–412. https://doi.org/10.1108/ec-12-2019-0560.

[38] Z. Ullah, B. Ullah, W. Khan, and S. ul Islam. Proportional topology optimisation with maximum entropy-based meshless method for minimum compliance and stress constrained problems. *Engineering with Computers*, **38**, (6), (2022), pp. 5541–5561. https://doi.org/10.1007/s00366-022-01683-w.

[39] H. Wang, W. Cheng, M. Zhang, R. Du, and W. Xiang. Non-gradient robust topology optimization method considering loading uncertainty. *Arabian Journal for Science and Engineering*, **46**, (2021), pp. 12599–12611. https://doi.org/10.1007/s13369-021-06010-x.

[40] M. N. Nguyen and T. Q. Bui. Multi-material gradient-free proportional topology optimization analysis for plates with variable thickness. *Structural and Multidisciplinary Optimization*, **65**, (3), (2022). https://doi.org/10.1007/s00158-022-03176-2.

[41] M. N. Nguyen, M. T. Tran, H. Q. Nguyen, and T. Q. Bui. A multi-material Proportional Topology Optimization approach for compliant mechanism problems. *European Journal of Mechanics - A/Solids*, **100**, (2023). https://doi.org/10.1016/j.euromechsol.2023.104957.

[42] R. Tavakoli and S. M. Mohseni. Alternating active-phase algorithm for multimaterial topology optimization problems: a 115-line MATLAB implementation. *Structural and Multidisciplinary Optimization*, **49**, (4), (2014), pp. 621–642. https://doi.org/10.1007/s00158-013-0999-1.

[43] M. N. Nguyen and T. Q. Bui. Concurrent multiscale topology optimization: A hybrid approach. *Vietnam Journal of Mechanics*, **44**, (3), (2022), pp. 266–279. https://doi.org/10.15625/0866-7136/17331.

[44] M. N. Nguyen and T. Q. Bui. A meshfree-based topology optimization approach without calculation of sensitivity. *Vietnam Journal of Mechanics*, **44**, (1), (2022), pp. 45–58. https://doi.org/10.15625/0866-7136/16679.

[45] M. T. Tran, M. N. Nguyen, T. Q. Bui, and H. Q. Nguyen. An enhanced proportional topology optimization with virtual elements: Formulation and numerical implementation. *Finite Elements in Analysis and Design*, **222**, (2023). https://doi.org/10.1016/j.finel.2023.103958.

[46] O. Sigmund. Morphology-based black and white filters for topology optimization. *Structural and Multidisciplinary Optimization*, **33**, (2007), pp. 401–424. https://doi.org/10.1007/s00158-006-0087-x.

[47] J. K. Guest, A. Asadpoure, and S.-H. Ha. Eliminating beta-continuation from Heaviside projection and density filter algorithms. *Structural and Multidisciplinary Optimization*, **44**, (2011), pp. 443–453. https://doi.org/10.1007/s00158-011-0676-1.

[48] L. Li and K. Khandelwal. Volume preserving projection filters and continuation methods in topology optimization. *Engineering Structures*, **85**, (2015), pp. 144–161. https://doi.org/10.1016/j.engstruct.2014.10.052.

[49] Y. Lu and L. Tong. Concurrent topology optimization of cellular structures and anisotropic materials. *Computers & Structures*, **255**, (2021). https://doi.org/10.1016/j.compstruc.2021.106624.

[50] B. Li, Y. Duan, H. Yang, Y. Lou, and W. H. Müller. Isogeometric topology optimization of strain gradient materials. *Computer Methods in Applied Mechanics and Engineering*, **397**, (2022). https://doi.org/10.1016/j.cma.2022.115135.

[51] S. Liu and W. Su. Topology optimization of couple-stress material structures. *Structural and Multidisciplinary Optimization*, **40**, (1-6), (2009), pp. 319–327. https://doi.org/10.1007/s00158-009-0367-3.

[52] N. Gan and Q. Wang. Topology optimization design related to size effect using the modified couple stress theory. *Engineering Optimization*, **55**, (1), (2021), pp. 158–176. https://doi.org/10.1080/0305215x.2021.1990911.